Fish scale containing alginate dialdehyde-gelatin bioink for bone tissue engineering

Biofabrication

PAPER

Fish scale containing alginate dialdehyde-gelatin bioink for bone tissue engineering

Aylin Kara Özenler[1,2,3], Thomas Distler[2], Funda Tihminlioglu[4] and Aldo R Boccaccini[2,*]

[1] Department of Bioengineering, İzmir Institute of Technology, İzmir 35433, Turkey
[2] Institute of Biomaterials, Department of Material Science and Engineering, Friedrich-Alexander-University Erlangen-Nuremberg, Erlangen 91058, Germany
[3] Center for Translational Bone, Joint and Soft Tissue Research, University Hospital Carl Gustav Carus and Faculty of Medicine, Technische Universität Dresden, Dresden 01307, Germany
[4] Department of Chemical Engineering, İzmir Institute of Technology, İzmir 35433, Turkey
[*] Author to whom any correspondence should be addressed.

E-mail: aldo.boccaccini@fau.de

Keywords: bioink, alginates, gelatin, fish scale, bone tissue engineering

Supplementary material for this article is available online

OPEN ACCESS

RECEIVED
26 September 2022

REVISED
11 January 2023

ACCEPTED FOR PUBLICATION
27 January 2023

PUBLISHED
15 February 2023

Abstract

The development of biomaterial inks suitable for biofabrication and mimicking the physicochemical properties of the extracellular matrix is essential for the application of bioprinting technology in tissue engineering (TE). The use of animal-derived proteinous materials, such as jellyfish collagen, or fish scale (FS) gelatin (GEL), has become an important pillar in biomaterial ink design to increase the bioactivity of hydrogels. However, besides the extraction of proteinous structures, the use of structurally intact FS as an additive could increase biocompatibility and bioactivity of hydrogels due to its organic (collagen) and inorganic (hydroxyapatite) contents, while simultaneously enhancing mechanical strength in three-dimensional (3D) printing applications. To test this hypothesis, we present here a composite biomaterial ink composed of FS and alginate dialdehyde (ADA)-GEL for 3D bioprinting applications. We fabricate 3D cell-laden hydrogels using mouse pre-osteoblast MC3T3-E1 cells. We evaluate the physicochemical and mechanical properties of FS incorporated ADA-GEL biomaterial inks as well as the bioactivity and cytocompatibility of cell-laden hydrogels. Due to the distinctive collagen orientation of the FS, the compressive strength of the hydrogels significantly increased with increasing FS particle content. Addition of FS also provided a tool to tune hydrogel stiffness. FS particles were homogeneously incorporated into the hydrogels. Particle-matrix integration was confirmed via scanning electron microscopy. FS incorporation in the ADA-GEL matrix increased the osteogenic differentiation of MC3T3-E1 cells in comparison to pristine ADA-GEL, as FS incorporation led to increased ALP activity and osteocalcin secretion of MC3T3-E1 cells. Due to the significantly increased stiffness and supported osteoinductivity of the hydrogels, FS structure as a natural collagen and hydroxyapatite source contributed to the biomaterial ink properties for bone engineering applications. Our findings indicate that ADA-GEL/FS represents a new biomaterial ink formulation with great potential for 3D bioprinting, and FS is confirmed as a promising additive for bone TE applications.

1. Introduction

Tissue engineering (TE) and regenerative medicine provide promising approaches to restore, replace or regenerate tissues. Numerous techniques have been used in TE applications to fabricate biomaterials, such as lyophilization, electrospinning, micropatterning, and three-dimensional (3D) printing. In recent years, 3D printing technology is being extensively investigated and considered a valid alternative for developing biomimetic patterns and 3D scaffolds with high precision [1].

3D-printed scaffolds that have been developed for TE approaches enable the delivery of cells or growth

factors to the damaged tissue or organ, as well as allowing mechanical support during the regeneration period [2]. Additive manufacturing (AM) technologies have been used to generate bio-engineered 3D structures to mimic the biological and functional complexity of the native tissues [3]. In biofabrication approaches, it is possible to create a 3D biological material by a computer-aided design and manufacturing process for patterning and assembling living materials with a prescribed 3D organization [4]. The printable material, called 'bioink' combines the biomaterial ink and cells or cell-based bioactive components which are essential for the regeneration of tissues. From a biological point of view, high water content hydrogels are attractive candidates for the incorporation of cells and bioactive compounds due to their aqueous 3D environment and adaptable chemistry, simulating the natural extracellular matrix [5]. In this context, biological materials and biopolymers provide a natural resource which can mimic the biochemical and proteinous properties of native tissues. Alginate, gelatin (GEL), collagen, chitosan, fibrin, etc, have been used in many TE applications [6–10]. In particular, alginate and GEL-based hydrogels are being extensively investigated in bioprinting applications due to their favorable printability and biocompatibility features [11, 12]. Besides the favorable properties of alginate for the printing process, such as biocompatibility and easy of crosslinking using divalent cations, it needs to be modified or combined with other materials due to a lack of cell adhesion motifs on the polymer backbone. Alginate dialdehyde (ADA), or oxidized alginate, is a derivative of alginate which can be synthesized via controlled chemical oxidation of sodium alginate using various oxidizing agents [13], and it provides functionality for further crosslinking via its aldehyde groups [14, 15]. Specifically, the aldehyde groups which are created during the oxidation reaction allow the alginate polymer to crosslink with amine-containing materials, such as proteins, via Schiff's base formation [16, 17]. GEL as a water-soluble protein derived from collagen, contains the Arg-Gly-Asp (RGD) peptide sequence, which is favorable for cell attachment [18]. Combining GEL and ADA leads to a promising hydrogel system for TE applications, which has shown 3D printability, high biocompatibility, and tunable degradation properties [11, 19–21]. Furthermore, enhanced printability of ADA-GEL has been engineered recently by heat treatment of GEL and optimum conditions were demonstrated for 3D printability [22].

For applications in bone TE, inorganic additives are commonly used to mimic the composite structure of bone tissue and to enhance the bioactivity of hydrogels [23–26]. As an example, hydroxyapatite is commonly used as an additive due to its biocompatibility, bioactivity and cell interaction [27]. Silica- and cellulose-based materials have been used as a filler material to support cellular activity and to enhance the mechanical stiffness of hydrogels [28–30]. Moreover, 3D-printed PCL and PLA struts were used to improve the mechanical stiffness of hydrogel-based scaffolds [31]. However, it is still a challenge to obtain a bioink formulation which provides both, high shape fidelity and cell viability in bioprinting applications. Organic and inorganic additives therefore have been used to improve the stiffness of the printed materials or to increase swelling capacity [32, 33]. Supporting cell viability during cell culture is in addition vital for the potential use of such fillers in regenerative clinical applications. Here we present the use of naturally derived fish scale (FS), which commonly is a waste product of the food industry, and investigate its use as a favorable source for collagen *and* hydroxyapatite in 3D bioprinting applications. As a relatively new biological derived material for TE and regenerative medicine, FS is a biocompatible and bioactive material and presents several advantages for bone TE applications [34, 35]. Similar to bone tissue, FS is composed of type I collagen and hydroxyapatite exhibiting a highly ordered 3D structure [36–38]. The distinctive arrangement of collagen fibrils layer by layer forms 3D micro-channels in different directions. Thus, multilayered microchannels provide a favorable surface morphology for cell attachment and growth, and also this arrangement is the major factor for mechanical strength [39–41]. Additionally, hydroxyapatite crystals, which are distributed through the aligned collagen fibers, serve as a biomineral source and allow for biomineralization of the structure [37]. Instead of using only inorganic or organic materials separately as additives, FS provides a multilayered 3D structure with both organic collagen fibrils and inorganic hydroxyapatite crystals. Previous studies have proven biocompatibility, bioactivity and biodegradability of FS as well as biologically safe extractable components [42, 43]. FS has been used previously in different TE applications such as wound healing, drug delivery, corneal regeneration, and has been mainly evaluated as a source for extraction of proteins for instance collagen and GEL as well as hydroxyapatite [34, 44–46]. However, the use of naturally derived FS without altering its structure has not been explored for 3D bioprinting before. Indeed, improvement of stiffness due to collagen fiber orientation, induction of mineralization by the hydroxyapatite content, and the biochemical similarity with bone tissue make FS a very attractive candidate for bone TE applications [36, 37, 39]. Therefore, utilization of FS in 3D bioprinting technology for bone TE is promising to better mimic bone tissue chemistry and mechanics. Previous studies have proven the high biocompatibility and bioactivity as well as the successful application of FS in bone TE [47–49]. It was

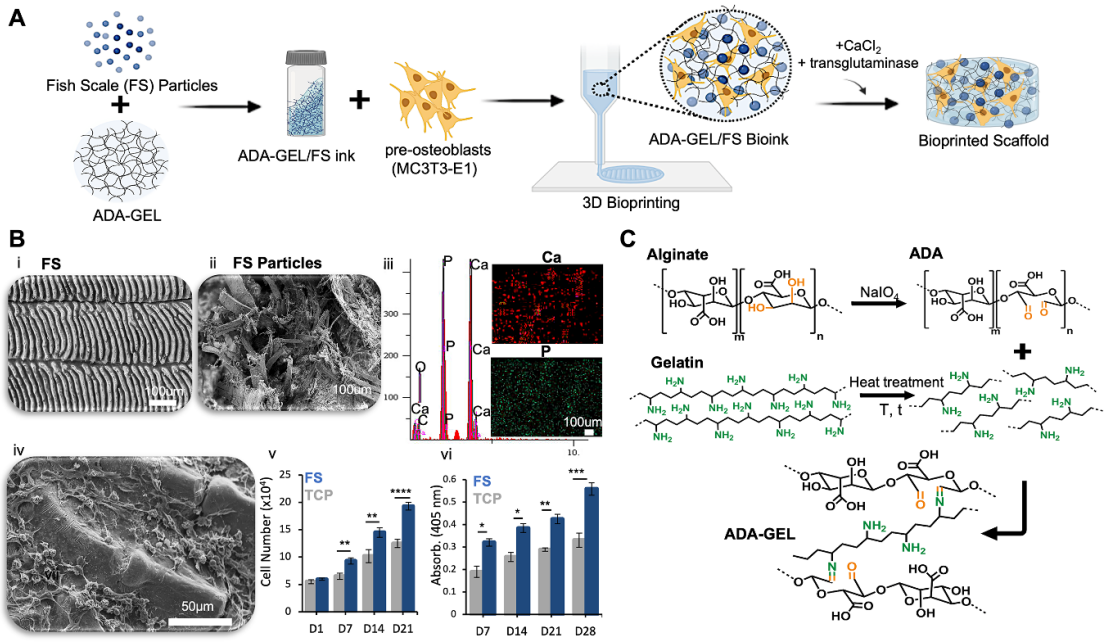

Figure 1. Schematic illustration of ADA-GEL/FS bioink containing pre-osteoblast MC3T3-E1 cells. (A) FS particles were homogeneously distributed into ADA-GEL matrix. Then MC3T3-E1 cells were mixed to obtain ADA-GEL/FS bioink. $CaCl_2$ and microbial transglutaminase (mTG) were used to crosslink the hydrogels via ionic, covalent and enzymatic crosslinking. (B) Characteristics of FS obtained from *Sparus aurata*: (i) SEM image of FS surface morphology shows highly ordered microchannels and (ii) FS particles after pulverization. (Scale bars: 100 μm). (iii) EDX analysis of FS particles show Ca, P, C, O concentration and elemental mapping analysis of Ca and P (Scale bar: 100 μm). (iv) SEM images of MC3T3-E1 cells seeded on FS after 21 d, indicating the cell-particle interaction. Scale bar: 50 μm. (High-magnification image can be seen in the supporting information, figure 1(C)). (v) PicoGreen proliferation and (vi) ALP activity assay results comparing FS and tissue culture plate (TCP) controls. All data are represented as mean ± SD. $^{*}p < 0.05$, $^{**}p < 0.01$, $^{***}p < 0.001$, $^{****}p < 0.0001$ indicate statistically significant differences. (C) Synthesis of ADA and preparation of the ADA-GEL hydrogel precursor. ALG oxidation with sodium meta periodate ($NaIO_4$) results in the cleavage of C–C bonds and the formation of aldehyde groups at the oxidized vicinal diols. Heat treatment of GEL to enhance printability, as described previously [22]. ADA and heat-treated GEL are mixed to induce reversible covalent imine bonds between GEL and ADA (Schiff base formation) [15].

reported that the mechanical strength as well as the biomineralization and osteogenic activity improved when FS particles were included in the structure [48, 50]. Boonyagul *et al* used GEL extracted from FS then blended with alginate to obtain biomaterial ink and evaluated its printability and physical properties as well as the viability of keratinocytes [51]. Different from the study of Boonyagul *et al*, we explore here the use of FS as a particle additive into ADA-GEL hydrogel. By this approach, we utilize both the collagen and hydroxyapatite composition of FS and carry out a comprehensive evaluation of the physicochemical properties, bioactivity, bioprinting capability and osteoinductive effects of the new bioink. Furthermore, in the literature, FS particles have not been combined with degradable and highly 3D printable ADA-GEL. Such approach could be an alternative way to enhance the bioactivity and osteoinductive properties of ADA-GEL for bone TE. The advantages of FS particles combined with biocompatible, highly printable ADA-GEL hydrogels [52] should provide better bioink formulations for 3D biofabrication, which has not been explored previously. Therefore, we present and characterize ADA-GEL/FS composite bioinks utilizing mouse pre-osteoblast cells (MC3T3-E1) for the 3D bioprinting study.

Thus, the study presented here (figure 1) focuses on the development of a new bioink composed of FS microparticles, ADA-GEL and MC3T3-E1 cells for bone TE applications (figure 1(A)). FS microparticles, which are natural sources for collagen and hydroxyapatite (figure 1(B)), were used as biocompatible additive and ADA-GEL was used as hydrogel matrix (figure 1(C)). Prepared ADA-GEL/FS composite bioink was bioprinted with MC3T3-E1 cells by using a 3D bioprinter. The potential application of the ADA-GEL/FS hydrogels for bone TE was evaluated by systematical investigation of their morphological, physicochemical, mechanical and biological properties.

2. Materials and methods

2.1. Materials

Sodium alginate from brown algae (VIVA Pharm, PH176) was purchased from JRS PHARMA GmbH & Co. KG (Germany). Dialysis tubing membranes (MWCO: 6–8 kDa) were from Repligen (Waltham, USA). GEL (gel strength 300, Type A) from porcine skin was obtained from Sigma Aldrich, Germany. Fishes (*Sparus aurata*) were obtained from a commercial dealer in İzmir, Turkey. All other

chemicals used in material synthesis were purchased from Sigma-Aldrich (Germany). Microbial transglutaminase (mTG) (Ajinomoto Co., Inc., ACTIVA WM, 85 − 135 U g^{-1}) and $CaCl_2$ (Sigma-Aldrich, Germany) were used for crosslinking process. MC3T3-E1 pre-osteoblasts (Sigma Aldrich, Germany) were used for cell culture study. Alpha modified minimum essential medium (α-MEM, Gibco, Life Technologies TM, Germany) were used as culture medium and all supplements L-glutamine, Fetal Bovine Serum (FBS), penicillin-streptomycin were purchased from Sigma Aldrich, Germany. For cell viability and cytotoxicity determination, water-soluble tetrazolium salt WST-8 solution (Cell Counting Kit-8, Sigma Aldrich, Germany) and LDH kit (Tox7 Toxicity kit, Sigma Aldrich) were used, respectively. Cell proliferation was quantified using the double-strand DNA (dsDNA) by Quant-iT PicoGreen ds-DNA Assay-Kit (Invitrogen, Life Technologies, Thermo Fisher, USA). Calcein acetoxymethyl ester (Calcein AM), and propidium iodide (PI) (Invitrogen, Molecular probes by Life technologies, USA) were used for Live/Dead staining assay. DAPI (4′,6-diamidino-2-phenylindole, Invitrogen, USA) was used for additional nuclease staining. Osteogenic differentiation was assessed with *Alkaline phosphatase* (ALP) activity (Biovision Inc. USA) and Osteocalcin (OC) secretion (Osteocalcin ELISA Kit, Abcam) assays.

2.2. Preparation of FS particles

FS were harvested from *Sparus aurata* and washed with distilled water five times. Decellularization of the FS was performed by adapting a protocol described previously [48, 50]. Initially, FS were incubated in a 10 mM Tris-HCl buffer and 0.1% EDTA at 4 °C for 24 h. To remove the cellular component from FS, 0.1% SDS in the Tris-HCl buffer was used at 4 °C for 3 d. Then, FS were rinsed with 70% ethanol for sterilization and stored in phosphate-buffered saline (PBS) at 4 °C before further application. To obtain particles, FS were grinded by using a laboratory mixer and filtered with a 100 μm mesh diameter membrane filter.

2.3. Synthesis of ADA

Alginate was oxidized by controlled oxidation using sodium meta periodate ($NaIO_4$), as described previously [53]. Briefly, 10 g of alginate were dispersed in an ethanol-water mixture (100 ml, 50:50 v v^{-1}) and oxidized in the absence of light under continuous stirring for six hours after the addition of 9.375 mmol $NaIO_4$. The oxidation reaction was quenched by adding 10 ml of ethylene glycol and by further stirring for 30 min. The mixture was allowed to sediment for 10 min. The ethanol phase was decanted followed by the transfer of the remaining solution containing oxidized alginate (ADA) into the dialysis tubing membrane and dialyzed against ultrapure water (UPW, Milli-Q, Merck, Germany) for five days with daily water exchange to remove of excess periodate. After dialysis, the collected final ADA solution as a product was frozen for a minimum of 24 h at −20 °C and lyophilized using a freeze dryer (Alpha LD1-2 Plus, Martin Christ GmbH, Germany).

2.4. Cell culture and maintenance

MC3T3-E1 pre-osteoblasts (passage 10) were cultured in cell culture flasks (Sarsted, Nümbrecht, Germany) using alpha modified minimum essential medium (α-MEM) supplemented with 1% (v v^{-1}) L-glutamine, 10% (v v^{-1}) FBS and 1% (v/v) penicillin-streptomycin. The cells were cultured in an incubator at 37 °C in a humidified atmosphere of 5% CO_2 and 95% humidity. For bioink composition, a cell pellet was obtained; first, cells were washed with PBS and detached from the cell culture flask using 0.25% Trypsin-EDTA, then cell number was determined with the Neubauer chambers. MC3T3-E1 (5×10^6 cells ml^{-1}) cell pellets were prepared by centrifugation and gently mixed with the ADA-GEL/FS ink materials. 3D-bioprinted hydrogels were cultured in the same culture medium and the medium was refreshed twice a week during the cell culture period.

2.5. Bioink formulation

GEL (15% w v^{-1}) solution was prepared in UPW by pre-treating at 80 °C for 3 h to tailor its rheological properties for improved printability [22]. Pre-treated GEL solution was filtered using 0.22 μm syringe filters (Carl Roth, Germany) and stored at 4 °C until further use. ADA (7.5% w v^{-1}) was dissolved in PBS (Thermo Fisher, US) and filtered using a 0.22 μm syringe filter. Equal amounts of ADA and GEL solutions were mixed for 30 min (37 °C) to reach a final hydrogel precursor of 3.75%/7.5% ADA-GEL. FS particles were disinfected by exposing UV light for 1 h. After disinfection, FS particles (1%, 3%, 5% and 10% w/v) were mixed with the ADA-GEL precursor and stirred to ensure homogenous dispersion for 15 min at 180 rpm, followed by ultrasonication for 10 min. Cell pellets of MC3T3-E1 (5×10^6 cells ml^{-1}) were added to the ADA-GEL/FS hydrogel precursor and dispersed by gentle stirring prior to 3D-bioprinting. Final ADA-GEL/FS hydrogel precursors containing 1%, 3%, 5%, 10% FS, and cells, were prepared, and ADA-GEL with cells served as a control.

2.6. Bioprinting

3D cylindrical hydrogels were bioprinted in a sterile environment using a 3D extrusion bioprinter Bioscaffolder 3.1 (GeSiM, GmbH Germany). To stabilize the viscosity, the temperature of the cartridge holder was set as 30 °C. The ADA-GEL/FS hydrogel precursor was transferred into the cartridge, inserted in the holder, then extruded through the 400 μm nozzles

with a tip velocity of 10 mm s^{-1} and extrusion pressure 100–190 kPa. All samples were fabricated by ten layers with diameter of 10 mm and the layer height was set to 0.4 mm. The bioprinted ADA-GEL/FS hydrogel samples were crosslinked by immersing them in the crosslinking solution (10% w v^{-1} mTG in 0.1 M $CaCl_2$) for 15 min at room temperature (22 °C, RT). After crosslinking, cells were covered in maintenance cell culture medium and the well plate was placed in the incubator to return the cells to physiological environment (37 °C, 5% CO_2).

2.7. Rheological tests

The rheological properties of the ADA-GEL and FS incorporated ADA-GEL biomaterial inks were determined using a rheometer equipped with a plate-plate geometry with a diameter of 60 mm (Rheotest RN 4, Medingen, Germany). Shear sweep tests were carried out by constantly increasing the shear rate from 0 to 300 s^{-1} (increment of 0.1 s^{-1} per second) with a gap distance of 0.5 mm at 25 °C. To assess the structural recovery of the hydrogel, thixotropy tests were applied. The thixotropy test consisted of a 30 s transient phase, a 30 s loading phase, and a 120 s recovery phase. The precursor was subjected to deformation of 0.001 at 10 rad s^{-1} during the transient and recovery phases. All tests were carried out at 25 °C with five repeated samples and a gap size of 0.5 mm.

2.8. Printability assessment

The printability of the ADA-GEL/FS inks was determined by considering the printing accuracy using light microscopy (Stemi 508, Carl Zeiss, Germany). The images were processed using Image J software. Printability factor (*Pr*) in accordance with the pore circularity (*C*), pore perimeter (*P*), and pore area (*A*) was calculated using the following equation [54]:

$$\mathrm{Pr} = \frac{\pi}{4} x \frac{1}{C} = \frac{P^2}{16A}. \quad (1)$$

The uniformity of the printed scaffolds was determined using the uniformity factor U described by Soltan *et al*, which was the measured horizontal length of a printed hydrogel strut (*L*) divided by the theoretical horizontal length of a parallel printed struts (L_t) [52];

$$U = \frac{L}{L_t}. \quad (2)$$

2.9. Scanning electron microscopy (SEM)

To evaluate the surface morphology, pore structure and particle-polymer interactions, 3D-printed scaffolds were observed by SEM. Freeze-dried samples were coated with a gold layer under argon gas by using Emitech K550X before analysis, and SEM images were recorded with a scanning electron microscope (Quanta FEG, FEI, Thermo Fisher Scientific).

2.10. Chemical characterization

Attenuated total reflectance Fourier transform infrared spectroscopy (ATR-FTIR) was carried out with lyophilized hydrogel samples to evaluate the chemical composition of the ADA-GEL/FS scaffolds. Analysis was performed at a wavenumber range of 4000–400 cm^{-1} with a resolution of 4 cm^{-1} using a IRAffinity-1S FTIR unit (Shimadzu, Europa GmbH).

2.11. Swelling/degradation kinetics

The swelling/degradation properties of the hydrogels were evaluated by weight changes during 35 d of incubation. The samples were incubated in cell culture medium at 37 °C with 5% CO_2 and 95% relative humidity, and the medium was refreshed every 48 h. The samples ($n = 6$) were immersed into the medium and weighed after carefully removing the excess medium at each time point. The initial mass of the samples before immersion in medium (m_i) and the current weight at each time point (m_c) was recorded. Swelling and degradation were calculated in weight % by the following equation:

$$\text{swelling}\,(wt\%) \text{ or degradation}\,(wt\%) = \left(\frac{m_c - m_i}{m_i}\right) x\ 100. \quad (3)$$

2.12. Mechanical characterization

The mechanical properties of the hydrogels were evaluated by uniaxial compression test using a universal testing system (Instron 3300 Floor Model, Instron® GmbH, Germany) equipped with a 100 N load cell in accordance with previously described methods [55]. The tests were performed at 1 mm min^{-1} crosshead speed until 15% strain at room temperature (22 °C) using cylindrical hydrogel specimens ($n = 6$, *diameter* = 7.5 mm, *height* = 3 mm). The initial elastic moduli of the hydrogels were determined for all groups as the slope in the linear-elastic deformation region from compressive stress–strain data between 5% and 10% deformation. Stress-relaxation time of the samples was defined as the time after which 50% of the initial stress dissipated in the samples.

2.13. Bioactivity study

The bioactivity of ADA-GEL/FS hydrogels was determined in simulated body fluid (SBF) during 28 d of incubation. SBF solution was prepared according to Kokubo and Takadama's study and as stated in ISO 23 317 (ISO 23 317:2014) [56]. 3D-printed scaffolds were immersed in SBF and placed in a shaking incubator (Heidolph Unimax 1010, Heidolph Instruments, Germany) at 37 °C and 90 rpm. The samples ($n = 4$) were incubated for 28 d and the SBF solution was refreshed every 2 d. The chemical composition of the scaffolds was determined by ATR-FTIR

(IRAffinity-1S, Shimadzu, Europa GmbH). The surface of the scaffolds was observed by SEM to determine the possible formation of apatite crystals and elemental analysis was performed using an EDX system attached to SEM (Quanta FEG FEI, Thermo Fisher Scientific).

2.14. *In vitro* evaluation of the bioprinted ADA-GEL/FS hydrogels

2.14.1. Cell viability

Cell viability was determined by water-soluble tetrazolium salt (WST-8) assay based on the conversion of water-soluble tetrazolium salt through cellular metabolism into the insoluble formazan. Bioprinted cell-laden hydrogels ($n = 6$) were cultured for 14 d and incubated with WST-8 solution for 3 h on days 1, 3, 7, and 14, followed by absorbance at 450 nm which was recorded using a plate reader (PHOmo, Anthos Mikrosysteme GmbH, Friesoythe, Germany).

2.14.2. Live/dead staining

The cellular viability in the 3D-bioprinted cell-laden hydrogels was determined by a Live/Dead staining assay. Initially, hydrogels were washed with Hank's balanced salt solutions (HBSS) and incubated with a staining solution containing 4 μl ml^{-1} Calcein AM and 5 μl ml^{-1} PI in HBSS for 45 min at 37 °C, 5% CO_2 in a humidified atmosphere. Cell nuclei were stained with 1 μl ml^{-1} DAPI for 5 min. After incubation, samples were washed with HBSS, and cell nuclei (blue), live (green) and dead (red) cells in the hydrogels were examined by fluorescence microscopy (AxioScope A.1, Carl Zeiss, Germany). After imaging, cells were counted using the cell counter plugin of the ImageJ. Cell viability was determined by calculating the ratio of the number of live cells to the total number of cells.

2.14.3. Extracellular lactate dehydrogenase (LDH) release assay

The potential cytotoxicity was determined using the LDH kit. Cell culture medium was collected for all groups ($n = 6$) and mixed with substrate solution, LDH cofactor solution, and dye solution into the cuvettes. After 30 min incubation of the samples in the dark, the absorbance at 490 and 690 nm was recorded using a UV–vis spectrophotometer.

2.14.4. PicoGreen assay

The proliferation of cells was quantified based on the dsDNA by Quant-iT PicoGreen Assay-Kit. 3D-bioprinted ADA-GEL/FS hydrogels ($n = 6$) were incubated for a 28 d of culture period. The samples were washed with PicoGreen assay buffer then mixed with a working solution and incubated for 5 min at room temperature in the dark. The relative fluorescence was recorded using a CFX connect spectrofluorometer (Bio-Rad, Germany).

2.14.5. ALP activity

Bioprinted ADA-GEL/FS cell-laden hydrogels were cultured in osteogenic (OS+) differentiation medium (α-MEM, 10% FCS, 1%penicilin/streptomycin, 50 μg ml^{-1} ascorbic acid, 10 μl ml^{-1} β-glycerophosphate, 100 nM dexamethasone) and non-osteogenic (OS-) medium (α-MEM, 10% FCS, 1%penicilin/streptomycin, 1 μl ml^{-1} L-glutamine) for 28 d. ALP activity was quantified on days 7, 14, 21, and 28 by colorimetric assay according to the manufacturer's protocol (Biovision Inc. USA). The absorbance at 405 nm was recorded by a plate reader (Varioskan Flash, Thermo Fisher Scientific).

2.14.6. OC secretion

The bioprinted cell-laden hydrogels were cultured in +OS and −OS media and the OC secretion was determined after 14, 21, and 28 d. Cell culture supernatants were collected for each time point and prepared according to the manufacturer instructions (Osteocalcin ELISA Kit, Abcam). Optical density at 450 nm was recorded (Varioskan Flash, ThermoFisher Scientific) and OC concentrations were determined by interpolating from the standard curve.

2.15. Statistical analysis

All data are expressed as mean ± standard deviation (SD). Each experiment was carried out with at least $n = 6$ individual samples if not otherwise noted. The differences between groups in biochemical and biomechanical tests were analyzed using a one-way analysis of variance (ANOVA) with Tukey's multiple comparison test. All p-values less than 0.05 were considered to be significant ($p < 0.05$).

3. Results & discussion

3.1. 3D-printed ADA-GEL/FS hydrogels

3D bioprinted ADA-GEL/FS hydrogels containing 1%, 3%, 5%, and 10% (wt %) FS particles were fabricated easily in a circular shape with ten layers. Figures 2(A)–(C) revealed optimization of the filament formation, printed ADA-GEL/FS structure, and printed hydrogel structures after crosslinking by using $CaCL_2$ and mTG, respectively. Light microscopy images of the printed structures demonstrate that all groups have shape fidelity and square-shaped macropores between the strands. The pure ADA-GEL hydrogels were optically transparent however the opacity of the composite hydrogels was increased depending on the FS particle concentration (figure 2(C)). Printability of the ADA-GEL/FS was assessed in terms of *Pr* factor, *U* factor, pore size, and strand diameter. In all groups, 3D printed hydrogels exhibited a square pore shape and *Pr* values were approximately one, indicating an ideal printability feature [54] (figure 2(D)). The

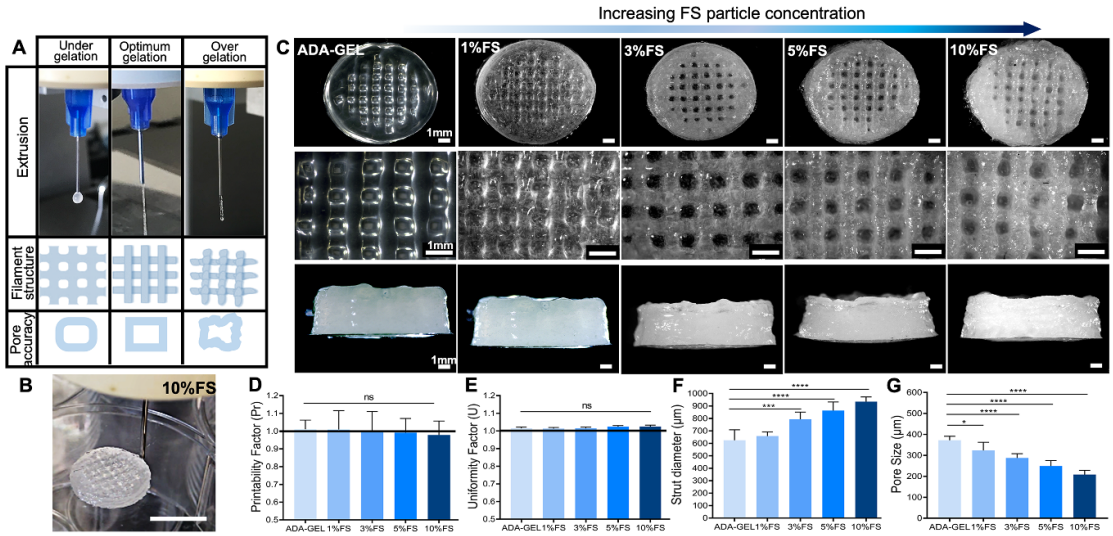

Figure 2. Fabricated 3D-printed ADA-GEL, ADA-GEL/1% FS, ADA-GEL/3% FS, ADA-GEL/5% FS, and ADA-GEL/10% FS composite scaffolds. (A) Optimization of filament formation for ADA-GEL/10% FS, with representative images of under-, optimal-, and over-gelation, as well as structural schematics of 3D-printed scaffolds. (B) Representative images of ADA-GEL/10% FS scaffold during the printing process (supporting information video 1). Scale bar: 10 mm (C) Light microscopy images of the 3D-printed ADA-GEL/FS scaffolds in top and side view after crosslinking. Scale bars: 1 mm. (D)–(G) Printability assessments of the ADA-GEL/FS scaffolds ($n = 6$), (D) Printability factor, (E) Uniformity factor, (F) strut diameter, and (G) pore size of the scaffolds. $^{*}p < 0.05$, $^{**}p < 0.01$, $^{***}p < 0.001$, and $^{****}p < 0.0001$ indicate the statistically significant differences of means in comparison to 3D-printed scaffolds by one-way ANOVA tests.

uniformity of the printed hydrogels has shown similarity without any significant differences (figure 2(E)). The strut diameter of the printed structures significantly increased with an increasing particle concentration (figure 2(F)). The strut diameters of the ADA-GEL and 1% FS containing hydrogels were similar to 650 ± 35 μm. The highest strut diameter was measured as 935 ± 32 μm in the 10% FS group with statistical differences compared to the other groups (figure 2(F)). Besides, pore sizes of the fabricated scaffolds were decreased with increasing FS concentrations (figure 2(G)). According to all printability assessments, all groups demonstrated uniform strut with square pore morphology, therefore ADA-GEL, ADA-GEL/1% FS, ADA-GEL/3% FS, ADA-GEL/5% FS, and ADA-GEL/10% FS composite formulations are acceptable as a new bioink composition. Regarding the printability results, pre-treatment of the GEL before mixing the ADA, and particles allowed easy fabrication and stable shape fidelity. Kreller *et al* showed the effect of pre-treatment of GEL at different temperatures in ADA-GEL hydrogels. It was reported that the most favorable printability characteristics with high shape fidelity was reached by preheating GEL at 80 °C, which provided a hierarchical microstructure [22]. Compared to the result of Kreller *et al*, similar Pr (∼1) and *U* factor (1.03 ± 0.05) were found in ADA-GEL hydrogels. In addition, incorporation of FS particles did not change the *Pr* and *U* factor despite the increasing strand size with decreasing pore size in the higher FS concentration group (ADA-GEL/10% FS). Moreover, it was estimated that the addition of FS did not affect the printability likely due to the elastic collagen fiber content of the particles [36]. With the enhancement of the printability by preheating the GEL and by the elasticity of FS, it was easy to fabricate hydrogel scaffolds by using a 3D printer.

Rheological tests of the ADA-GEL and ADA-GEL/FS hydrogel precursors were performed to investigate the effect of FS particle addition on ADA-GEL viscosity and shear thinning behavior. The shear sweep test results indicated that viscosity decreased while the shear rate increased (supporting information, figure 4). The viscosity curves revealed that complex viscosity increased with the addition of FS (supporting information, figure 4). The viscosity at rest was obtained from the average of the first measurement point (at a shear rate of 1 s^{-1}) and indicated that viscosity increased with an increasing FS amount in the ADA-GEL precursors. Viscosity at 1 s^{-1} shear rate was measured as ∼66, and ∼77 Pa s for ADA-GEL and ADA-GEL/1% FS hydrogel precursors, respectively. With increasing FS content the viscosity increased with a statistically significant difference, e.g. when comparing 3% FS (∼95 Pa s), 5% FS (∼165 Pa s) and 10% FS (∼232 Pa s) groups. All prepared materials exhibited a shear-thinning behavior which indicates that all materials have extrusion-printing capacity. Thixotropy test showed structural recovery of the materials and all hydrogel precursors showed self-recovery properties. The thixotropic behavior of ADA-GEL and 1% FS containing groups was similar, however higher FS content groups exhibited increased recovery behavior, notably 10% FS containing ADA-GEL hydrogel precursors exhibited the highest recovery behavior (supporting information, figure 4).

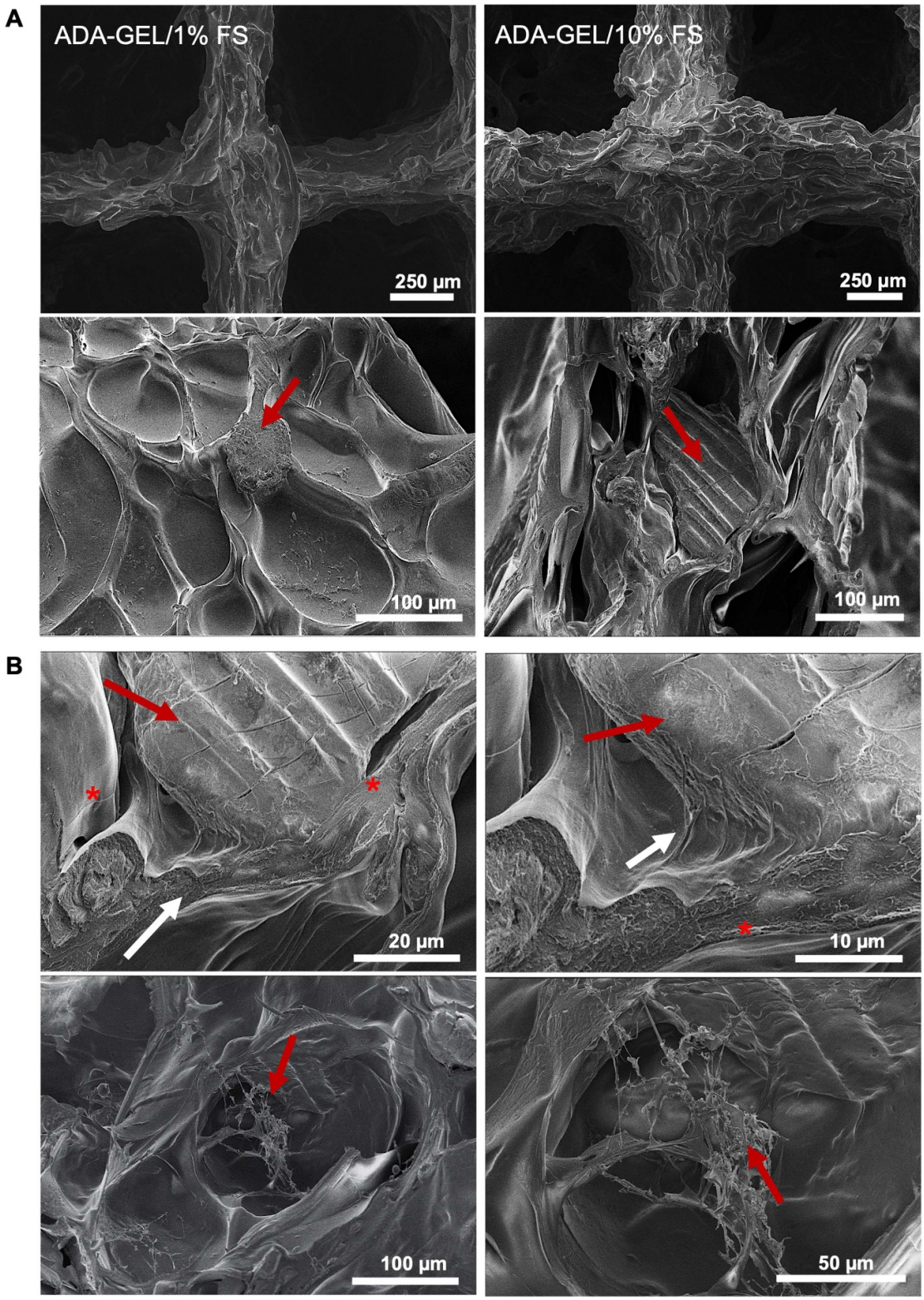

Figure 3. 3D-printed FS reinforced ADA-GEL scaffolds. (A) SEM images of the ADA-GEL/1% FS and ADA-GEL/10% FS scaffolds show the surface morphology of the scaffolds on the top view. The bottom images display FS particles (indicated with red arrows) incorporated into the ADAGEL matrix. Scale bars: 250 μm (1st top), 100 μm (2nd bottom). (B) FS particles and ADA-GEL interactions (white arrow) show good incorporation of FS into the polymer matrix (red asterisk). In the bottom images, red arrows indicate the fibrillar structures of FS. Scale bars: 20 μm, 10 μm (top right and left), 100 μm, 50 μm (bottom right and left).

To evaluate the morphology of the scaffolds and the particle-polymer interaction in the printed structures, SEM was carried out. Micrographs showed that the incorporation of FS particles in the ADA-GEL matrix increased the roughness of the surface (figure 3(A)). The surface morphology of the scaffolds was changed by increasing particle concentration and incorporation into the ADA-GEL

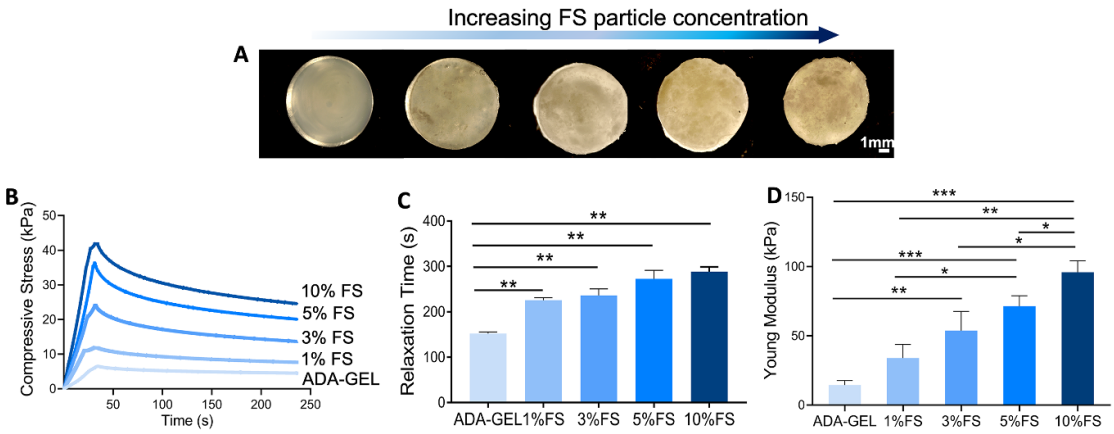

Figure 4. Mechanical properties of 3D-printed ADA-GEL, ADA-GEL/1% FS, ADA-GEL/3% FS, ADA-GEL/5% FS, and ADA-GEL/10% FS composite hydrogels. (A) Light microscopy images of the hydrogels with an increasing particle content prepared for mechanical test (scale bars: 1 mm). (B) Compressive stress over time. (C) Stress relaxation time is defined as the time after which 50% of the initial stress (upon 15% initial displacement) dissipated, and (D) Young's modulus of the ADA-GEL/FS hydrogels. All data are represented as mean ± SD. The measurements were performed using six sample replicates ($n = 6$). $^{*}p < 0.05$, $^{**}p < 0.01$, $^{***}p < 0.001$ indicate statistical differences of means in comparison to pristine ADA-GEL and FS incorporated ADA-GEL hydrogels by one-way ANOVA test.

structure (supporting information figure 2). The collagen content of FS particles as well as their fibrillary structure could affect the surface morphology leading to increased surface roughness. FS particles are easily seen on the composite scaffolds by SEM images with their distinctive morphology (figure 3(A) (bottom)). For the detailed investigation of the particle-polymer interaction cross-sectional areas were observed by SEM. Images showed that particles well integrated within the ADA-GEL matrix and FS particles were seen as embedded in the structures figure 3(B)). The areas where particles interact with ADA-GEL and the fibrous structure of the particles in the structure are demonstrated in figure 3(B). The identical chemical composition of GEL and collagen allows good interaction between ADA-GEL and FS particles with proper interface interaction.

3.2. FS particles addition improves the mechanical properties

The mechanical properties of FS incorporated ADA-GEL hydrogels were investigated by stress-relaxation tests. Light microscopy images of the hydrogels prepared for mechanical tests are shown in figure 4(A). Test results showed that ADA-GEL has the lowest stiffness and Young̀s modulus as well as relaxes the fastest. FS incorporation into ADA-GEL matrix significantly enhanced the stiffness providing a composite structure, as confirmed by SEM images (figure 4(B)). A higher compressive stress was found in the 10% FS incorporated group compared to the other groups. Figure 4(C) showed the stress relaxation time defined as the time after which 50% of the initial stress dissipated in the samples [55]. The stress–relaxation of the hydrogels was improved significantly with increasing particle concentration. The Young's modulus of the hydrogels was quantified by fitting a slope in the linear elastic deformation region from stress–strain data between 5% and 10% deformation. It was measured that the Young's modulus of the hydrogels increased according to the particle concentration, the higher modulus was recorded as 96 ± 8 kPa in ADA-GEL/10% hydrogels and there is a statistical difference compared to the other groups (figure 4(D)). Incorporation of FS particles into the ADA-GEL matrix significantly increased the Young's modulus of the ADA-GEL. Collagen fiber composition and orientation of FS could lead to this improvement. Ikoma *et al* demonstrated collagen fiber orientation in the FS microstructure affecting the mechanical strength of the FS particles [36]. It was found that the high tensile strength of the FS can be attributed to the highly ordered collagen fibers in association with long, narrow apatite crystals that are aligned along the crystallographic plane parallel to the collagen fibers [36, 37]. The alignment of apatite crystals in ordered collagen biomatrices not only serves as an inorganic binder to strengthen the tissue but also provides functional advantages based on mechanical anisotropy. Due to these collagen fibers and apatite crystals arrangement, FS particles show also flexibility [36, 37], therefore FS particles have great advantages as a reinforcement material in polymer matrices. In addition, ADA-GEL represents an ideal polymer matrix to incorporate FS, therefore, the proper particle-polymer integration provides load transfer between the two materials, and the mechanical strength of the hydrogels could be increased and tuned by using FS particles.

3.3. Tunable swelling properties with the addition of FS

Physicochemical properties of FS incorporated ADA-GEL scaffolds were evaluated by FTIR analysis, swelling and degradation studies. FTIR absorbance spectra

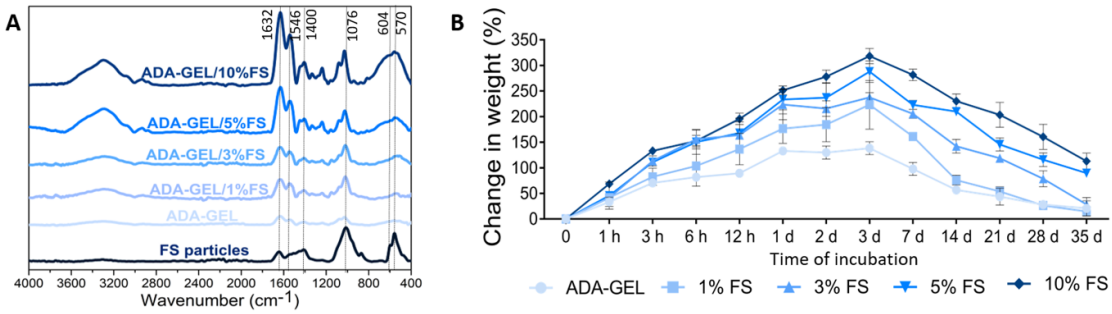

Figure 5. Physicochemical properties of 3D-printed ADA-GEL, ADA-GEL/1% FS, ADA-GEL/3% FS, ADA-GEL/5% FS, and ADA-GEL/10% FS composite scaffolds. (A) FTIR spectrum of FS particles, ADA-GEL and FS incorporated ADA-GEL scaffolds ($n = 4$). (B) Swelling/degradation behavior of the scaffolds during 35 d incubation period in cell culture medium. Measurements were performed using six replicates of samples ($n = 6$) and data represented as mean ± SD.

of FS particles, ADA-GEL and FS incorporated ADA-GEL scaffolds displayed the formation of absorbance peaks in figure 5(A). The main characteristic absorption bands of collagen including C=O peptide group of amide I, N–H bending vibration and C–N stretching vibration of amide II and C–C stretching vibrations of amide III, were observed at 1632 cm^{-1}, 1546 cm^{-1} and 1400 cm^{-1}, respectively. P–O bending bands around 604 and 570 cm^{-1} are assigned to the apatite crystals [36]. The main characteristic peaks from both collagen and apatite increased for FS incorporated ADA-GEL scaffolds with increasing particle concentration. Moreover, the main characteristic peaks of ADA-GEL were detected in all scaffold groups. Amide I (1630 cm^{-1}), amide II (1540 cm^{-1}) bands of polypeptides and proteins from GEL and amide III (1440 cm^{-1}) bands of carboxylate salt groups from ADA were detected in broadened peaks in the ADA-GEL/FS scaffold groups [57].

The swelling and degradation behavior of the ADA-GEL/FS scaffolds was evaluated by measuring the weight gain/loss during 35 d of incubation in cell culture medium (figure 5(B)). All printed scaffolds were swollen for three days, and the addition of FS particles increased the swelling properties of the structures. ADA-GEL showed the lowest swelling behavior compared to FS incorporated groups. Swelling of the ADA-GEL samples was detected for up to 150% for three days, similar to the previous study [14]. The swelling capacity was increased with the addition of FS particles. The highest swelling was measured in the 10% FS group, with a 350% weight gain, which could be due to the highly hydrophilic collagen fibers in the FS particles [58]. Feng *et al* obtained collagen powder extracted from FS and demonstrated swelling capacity of hydrogels composed of ADA and aminated FS collagen for wound healing applications [59], obtaining similar results (over 400%)[59]. After seven days of incubation, mass loss was observed in all groups. The ADA-GEL and 1% FS groups showed a similar degradation behavior, and weight lost was detected after 35 d. ADA-GEL containing 3%, 5% and 10% FS composite scaffolds remained in a swollen state and were stable over 35 d without a significant weight loss. Notably, for 5% and 10% FS groups a swelling of 300% was observed. ADA-GEL/FS scaffolds remained stable throughout the 35 d incubation period. This stability might be due to the crosslinking of the ADA-GEL/FS after printing. Ionically and covalently crosslinking with $CaCl_2$ and mTG allows the 3D-bioprinted scaffolds to remain stable for the 35 d incubation period.

3.4. ADA-GEL/FS composition increases bioactivity

The bioactivity of the ADA-GEL/FS scaffolds was assessed by SEM, EDX, and FTIR analysis. Figure 6(A) depicts the apatite formation on the surface of the ADA-GEL/10% FS scaffold after 28 d of incubation in SBF. EDX analysis confirms the Ca-P layer formation on the surface of the scaffold showing the calcium (Ca), oxygen (O), and phosphorus (P) elements on the surface of the formed layer (figure 6(B)). FTIR absorbance spectra of ADA-GEL and ADA-GEL/FS scaffolds showed absorbance peaks at 1013, 600, and 555 cm^{-1} after 28 d of incubation in SBF (figure 6(C)). The increasing intensity of the 1010, 550, and 600 cm^{-1} peaks is indicative of carbonate and phosphate formation on the surface of the composite scaffolds. Combining the SEM, EDX and FTIR results, it can be confirmed that ADA-GEL/FS hydrogels are bioactive, and bioactivity increased the Ca-P formation with the addition of FS particles. FS particles have biomineralization properties due to the hydroxyapatite content [37]. Therefore, the use of the whole FS structure without extraction of any component supports the bioactivity of the hydrogels. Unlike studies that use collagen or GEL extracted from FS separately, we evaluated and demonstrated the bioactivity characteristics of ADA-GEL/FS samples [51].

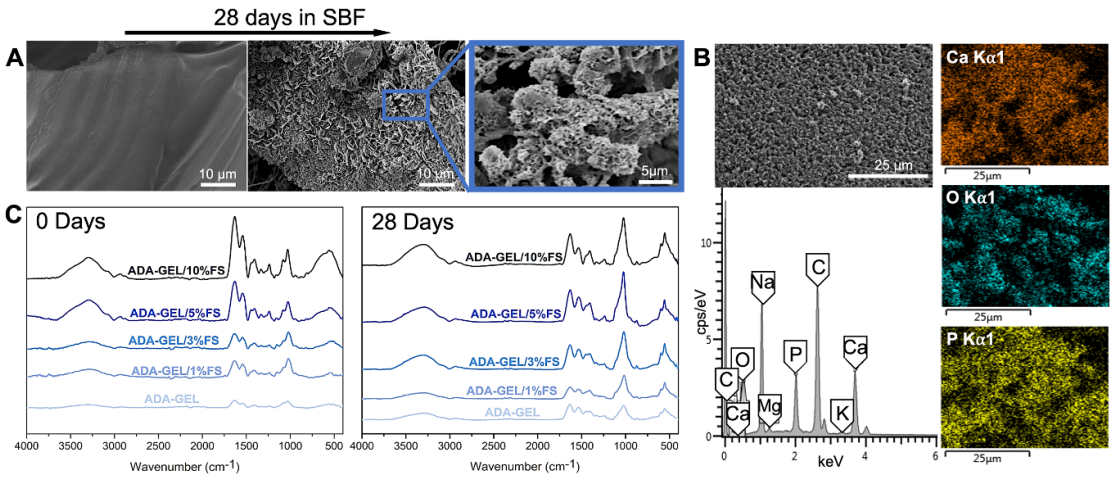

Figure 6. Bioactivity study of ADA-GEL/FS composite scaffolds. (A) SEM images of 3D printed ADA-GEL/10% FS scaffolds before (left) and after (right) incubation in SBF for 28 d. Scale bars: 10 μm. (B) EDX spectrum of ADA-GEL/10% FS scaffolds incubated for 28 d in SBF, indicating the formation of calcium, phosphorus and oxygen on the scaffold layer. Scale bar: 25 μm. (C) FTIR analysis of ADA-GEL, 1%, 3%, 5%, and 10% FS scaffolds after 0 and 28 d of incubation in SBF.

3.5. ADA-GEL/FS hydrogels allow cell proliferation with high cell viability

In vitro cell culture studies were performed to investigate the viability, morphology, proliferation, and bioactivity of the MC3T3-E1 pre-osteoblasts in biofabricated ADA-GEL/FS composite hydrogels. The viability of the cells was assessed by Live/Dead staining assay and staining results demonstrated that cells survived and maintained their viability in FS incorporated bioink compositions after 14 d (figure 7(A)). Live cells (green) spread and covered the surface of the hydrogels, and a few dead cells (red) were observed during the cell culture period even in the late stages of cultivation. In addition, cell viability was determined over 90% (figure 7(B)) which indicates that the bioink composition is biocompatible and ideally appropriate for cell growth. According to the cell culture assays, MC3T3-E1 preosteoblasts maintained viability without any cytotoxic effect for 14 d of culture (figures 7(C) and (D)). Extracellular LDH assay results confirmed that the 3D bioprinted hydrogels are not toxic (figure 7(C)). Also, cell viability assay results showed an increasing trend during the cell culture period and higher viability was found in 10% FS incorporated ADA-GEL hydrogels with statistical differences when compared to the other group (figure 7(D)). The composition of FS provides favorable characteristics for bone TE due to its collagen and hydroxyapatite content. Biocompatible features of ADA-GEL and the favorable RGD sequence of GEL promote cell proliferation, and furthermore, the 3D distinctive microchannel structure of FS allows cells to grow and migrate inside the structure [40, 50]. Additionally, it was observed that FS is non-toxic and human osteoblast cells attached, proliferated, and spread on the surface of FS while maintaining their viability (figure 1(B), Supporting information figure 1(C)). With a similar biochemical composition to bone, FS incorporated hydrogels thus showed cytocompatibility and supported cell growth.

The 3D-bioprinted hydrogels were observed during the cell culture period by light microscopy (figure 8(A)). MC3T3-E1 preosteoblast cells were observed inside the composite hydrogels. Moreover, FS particles are seen as rod-shaped structures. After 14 d of culture, cells were observed around the pore structures, especially at higher FS concentrations of ADA-GEL/FS hydrogels. Figure 8(B) depicted that cells attached and proliferated around the pores of the scaffolds and grew until covering the pore area for 21 d. This cell behavior indicates that cells could migrate and grow through the surface of the hydrogels which proves that ADA-GEL/FS bioink composition is not cytotoxic. The cells moved out from the hydrogel and started covering and growing on the surface of the ADA-GEL/FS hydrogel matrix in a favorable biocompatible environment. In addition, PicoGreen proliferation assay results confirmed cell proliferation during the 28 d of incubation period as seen in figure 8(C). FS incorporation enhanced cell proliferation when compared to the pure ADA-GEL hydrogels. Notably, 3% FS, 5% FS and 10% FS groups showed higher proliferation and statistical differences were found in comparison to the ADA-GEL and ADA-GEL/10% FS hydrogels. Besides, significant differences were found between day one and day 28 in all scaffold groups. The biocompatible polymer combination of ADA-GEL is capable of inducing cell proliferation as proven previously [60]. Additionally, the swelling capacity of hydrogels demonstrated in figure 5(B) could also support cell proliferation. The increasing trend in cell viability and proliferation might also be due to the high amino acid content of FS as FS is mainly composed of collagen fibers [61, 62].

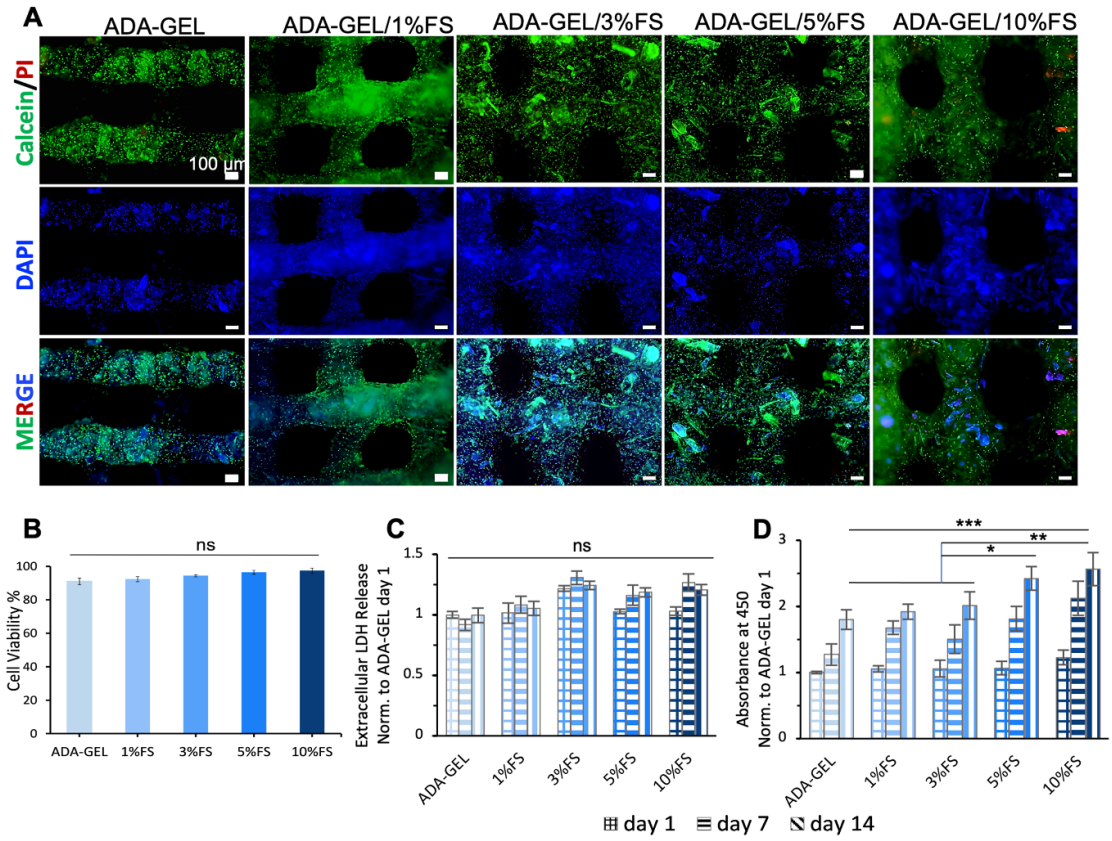

Figure 7. Cytotoxicity assessment of neat ADA-GEL and FS incorporated ADA-GEL cell-laden hydrogels. (A) Live/Dead assays of MC3T3-E1 cells inside and on the top of the bioprinted hydrogels for 14 d of incubation. (Scale bars: 100 μm). Calcein AM (green), PI (red), and DAPI (blue) staining represent live, dead cells, and cell nuclei respectively. (B) Total cell viability is expressed as a ratio of the viable cells to total cell numbers quantified from the fluorescence images on 14 d, ($n = 5$). (C) Possible toxicity assessment by the quantification of the extracellular LDH for 14 d ($n = 6$). (D) Cell viability assessment of MC3T3-E1 cells into bioprinted hydrogels ($n = 6$), normalized to ADA-GEL on 1st day of incubation. All data is represented as mean ± SD, $^{*}p < 0.05$, $^{**}p < 0.01$, $^{***}p < 0.001$ indicate statistically significant difference of means.

Besides, it was shown previously that FS collagen peptides induced cell proliferation as well as inhibited cytotoxicity showing the therapeutic potential of FS collagen [63].

3.6. Bioprinted ADA-GEL/FS hydrogels induce osteogenic differentiation

Elongated and spread cells on FS particles showing cell-particle interaction were observed by light microscopy (figure 9(A)) and Live/Dead staining (figure 9(B)). MC3T3-E1 cells were attached and proliferated both inside the polymer matrix and on the FS surface. Due to the favorable microenvironment of the ADA-GEL/FS hydrogels, cells intended to adhere to the structure and to grow inside the hydrogel matrix during the cell culture period.

Differentiation of MC3T3-E1 cells inside the 3D-bioprinted ADA-GEL/FS hydrogels was evaluated in terms of ALP activity (figure 9(C)) and OC secretion (figure 9(D)) during 28 d of culture period. It was observed that ALP activity increased in both +OS and −OS culture conditions, notably after 7 d of culture period and proceeded with an increasing trend for 28 d. The highest ALP activity was measured in the 10% FS group on day 28 with statistically significant differences compared to the other groups (figure 9(C)). The ALP activity of cells was quite increased with +OS induction, nevertheless, ALP activity was also detected in the -OS groups, especially in the 5% and 10% FS containing groups, which indicate the osteogenic capacity of FS particles. In -OS groups, the 10% FS containing group showed the highest ALP activity on days 21 and 28 with statistically differences compared to the other groups. In +OS groups, the highest ALP activity was found with statistical differences, especially on days 28, for all groups. The statistically significant differences were detected compared to the +OS and −OS groups. The addition of FS particles improved the ALP activity of cells with and without osteogenic induction. This increasing ALP activity shows that osteogenic differentiation could be promoted by the hydroxyapatite content of FS particles. Distinctive collagen and hydroxyapatite orientation of FS particles has a natural biomineralization capacity which supports osteogenic differentiation [37]. The results indicated that the ALP activity of cells inside the bioprinted hydrogels was improved by both +OS induction and by the addition of FS particles.

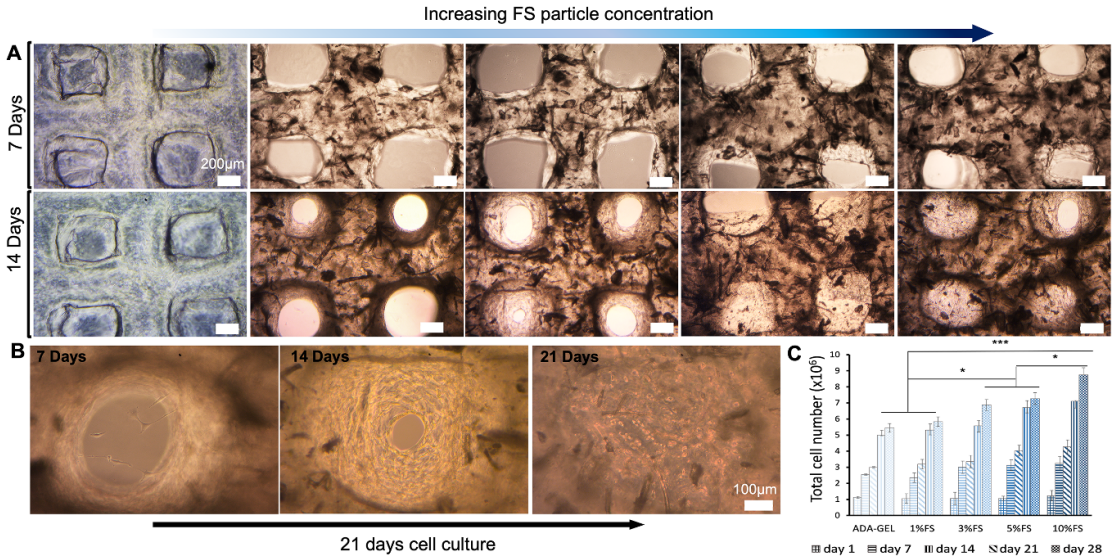

Figure 8. *In vitro* cytocompatibility assessment of the bioprinted hydrogels. (A) Light microscopy images of the bioprinted hydrogels after 7 and 14 d of incubation. (Scale bars: 200 μm) (B) Light microscopy images of MC3T3 cells localized around the pore where they grew until covering the pore area during 21 d of culture period. (Scale bars: 100 μm) (C) Cell proliferation assay showing the total cell number in the bioprinted hydrogels. All data is represented as mean ± SD. $^{*}p < 0.05$, $^{**}p < 0.01$, $^{***}p < 0.001$ indicate statistically significant difference of means.

OC is a bone-specific protein and is known as one of the important markers for osteogenic differentiation to act as a regulator for bone matrix mineralization [64]. Therefore, OC secretion was quantified to determine the differentiation of the cells into the hydrogels (figure 9(D)). The results indicated that OC secretion showed an increasing trend during the incubation period and secretion was improved depending on FS content in both +OS and −OS culture conditions. OC secretion of the cells in ADA-GEL hydrogels was stable at each time point in both -OS. However, FS incorporated ADA-GEL hydrogels increased during the culture period in −OS, notably on day 28. In +OS condition, OC secretion was significantly higher than in -OS condition on day 21 and 28. Statistically significant differences were found in comparison to −OS and +OS conditions. Besides, OC secretions increased on day 14 and on day 21 in FS containing groups with statistically significantly differences, and the 10% FS group exhibited the highest OC secretion on day 28 compared to the other groups. This increase could be associated with the hydroxyapatite and collagen content of FS particles demonstrated in a previous study [58]. Many studies have reported the support of osteogenic differentiation in presence of hydroxyapatite inside hydrogel structures [65–67]. The osteogenic differentiation capacity of FS without any osteogenic induction is another advantage for bone TE applications, e.g. FS particles provide a self-osteoinductive capacity to the biomaterial [37, 68]. Liu and Sun reported that the collagen extracted from FS particles has a capacity for osteogenic differentiation of BMSCs without any additional supplement [68]. In addition, it was demonstrated that FS incorporated in chitosan scaffolds induces the osteogenic differentiation of Saos-2 cells [50]. Our results support this suggestion by showing an increase in ALP and OC secretion without +OS induction in the medium using ADA-GEL/FS hydrogels. As hypothesis, the rich amino acid content of the FS particles due to collagen composition might be a source of growth factors which support osteogenic differentiation [69–71]. Moreover, our SEM data indicate the interaction between FS particles and ADA-GEL which results in an increased surface roughness and also enhanced stiffness of the FS incorporated ADA-GEL. The mechanical tests showed an increased stiffness when increasing FS particle content. Thus, osteogenic differentiation of the cells inside ADA-GEL/FS hydrogels might be additionally influenced by mechano-sensing of the cells and mechano-transduction. It was reported previously that a mechano-transduction mechanism triggers the osteogenic differentiation of human mesenchymal stem cells and preosteoblast cells [72–74], which is the ability of bone to sense and convert external mechanical stimuli into a biochemical response in the natural process of osteogenic differentiation. Several *in vitro* studies have demonstrated the intracellular and extracellular signaling components and pathways involved in mechano-transduction, such as integrins, cytoskeleton, ion channels, mitogen-activated protein kinase (MAPK) pathway, protein kinase A and C pathways (PKA, PKC) [75]. The effect of scaffold stiffness on osteogenic differentiation of dental pulp stem cells has been reported [76]. Increasing stiffness of the scaffolds (6, 16, 54, 135 kPa) influenced the cell behavior

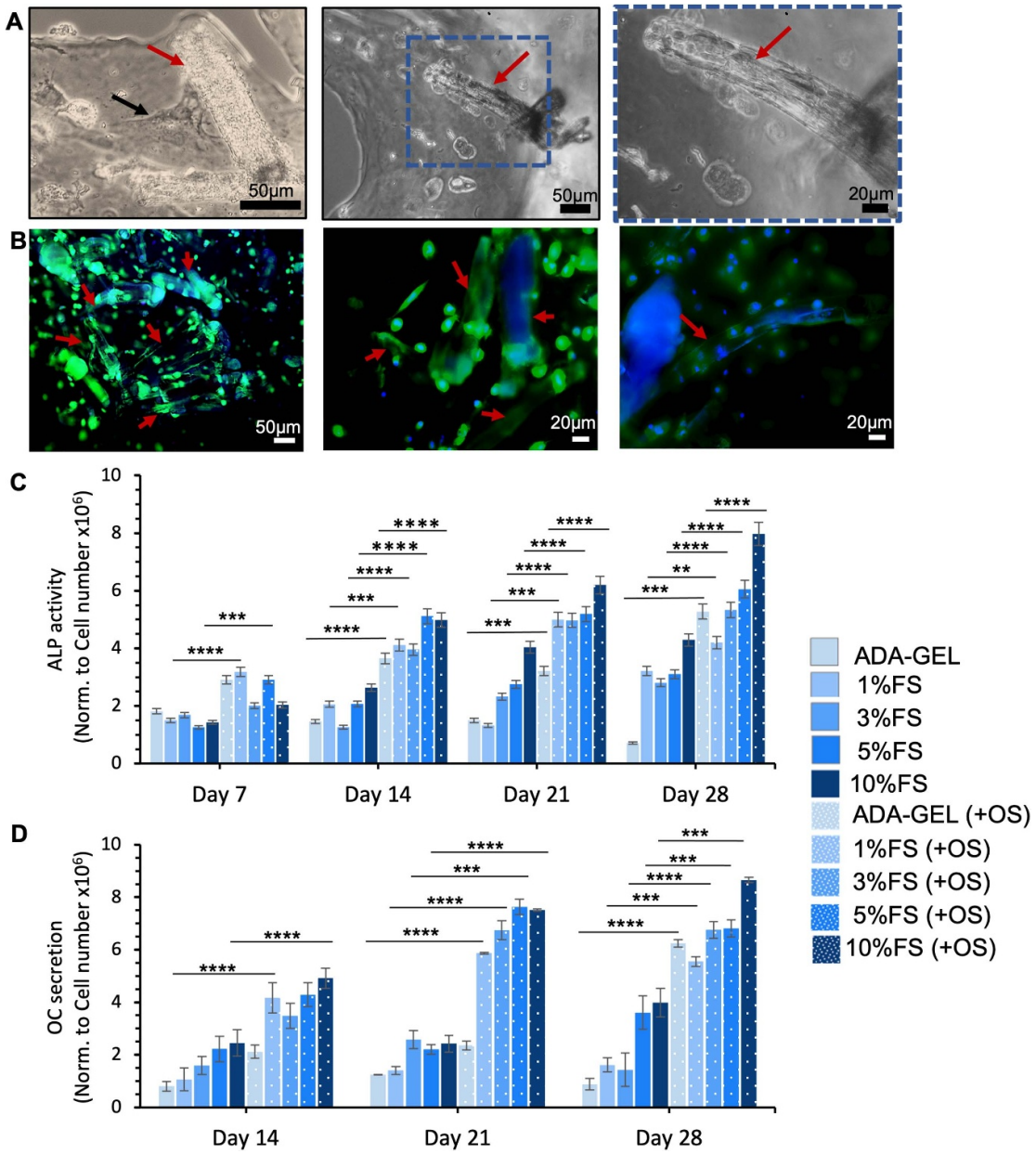

Figure 9. MC3T3-E1 cells and FS particle interaction inside the 3D bioprinted hydrogels and differentiation study of the ADA-GEL/FS bioprinted hydrogels. (A) Light microscopy images showing cell-particle interaction. Red and black arrows indicate FS and cells, respectively. (Scale bars: left to the right, 50 μm, 50 μm, 20 μm). (B) Live/dead staining images of the cells attaching and interacting with FS particles (red arrows) inside of the bioprinted hydrogels. Calcein AM (green); live cells, PI (red); dead cells, and DAPI (blue); cell nuclei. (Scale bars: left to the right, 50 μm, 20 μm, 20 μm). (C) ALP and (D) Osteocalcin secretion of the MC3T3-E1 cells in the 3D-bioprinted hydrogels ($n = 6$) cultured in osteogenic (+OS) and non-osteogenic medium. Data is represented as mean ± SD normalized to cell number. $^{**}p < 0.01$, $^{***}p < 0.001$ and $^{****}p < 0.0001$ indicate statistically significant difference of means.

and improved both cell proliferation and osteogenic differentiation as well as increased expression of ß-catenin and decreased GSK-3 ß has been observed, indicating the involvement of the osteogenic signaling pathway [76]. Another study reported that MC3T3-E1 cells cultured on stiffer substrates expressed higher levels of ALP, OC, and bone sialoprotein (BSP), as well as showing greater MAPK activity. In addition, inhibition of MAPK activity suppressed expression of OC and BSP, indicating that MC3T3-E1 cells undergo osteogenic differentiation through a MAPK-dependent mechanism [77]. Similar to the ALP results, OC quantification indicates that FS addition could promote osteogenic differentiation. Indeed the results of the present differentiation study revealed that 3D-bioprinted ADA-GEL/FS hydrogels induced cell differentiation. Also, both the natural biomineralization capacity of FS particles and +OS induction property supported the differentiation of MC3T3-E1 cells inside the ADA-GEL/FS hydrogels.

Additives used in hydrogels for 3D (bio)printing are intended to improve the structural composition, physicochemical properties, degradation profile, as

well as cell-material interactions. Previous studies have shown the effect of additives, such as nanoclay, bioactive glass, naturally derived collagen, etc, on hydrogels for 3D bioprinting applications. For instance, Ahlfeld *et al* reported 3D printable bioink composed of nanoclay additive, alginate and methylcellulose with high shape fidelity and demonstrated the protein releasing kinetics of the 3D bioprinted scaffolds by addition of bovine serum albumin (BSA) and vascular endothelial growth factor (VEGF) into the nanoclay containing bioinks [78, 79]. Cai *et al* reported nanoclay incorporated alginate-GEL hydrogels for potential 3D bioprinting applications and showed the printability of the composite biomaterial inks and increased swelling behavior by addition of the inorganic filler [25]. In another study, Heid *et al* reported the influence of the incorporation of bioactive inorganic particles (calcium silicate) in ADA-GEL bioinks on the stability of 3D printed scaffolds during 28 d of incubation [60]. In the present study, the effect of FS particles on ADA-GEL bioink characteristics was evaluated in terms of printability, and mechanical, physicochemical, cytocompatibility and osteoinductivity properties. With the addition of FS particles in the ADA-GEL matrix, cell-laden hydrogels were bioprinted successfully, mechanical stiffness was improved with the proper particle-polymer interaction, bioactivity was supported due to the biomineralization ability of FS particles and osteogenic activity was induced. As a result, the composite ADA-GEL/FS bioink formulation introduced in this study has potential for bioprinting applications and FS particles can be considered as a favorable dual collagen and hydroxyapatite additive for bone TE. The main focus of the current study was to develop and characterize 3D-printable cytocompatible bioinks with potential for bone TE using FS particles, which has not been demonstrated before in the same material combination. While the data demonstrate the cytocompatibility of ADA-GEL/FS bioink with differentiation capacity of pre-osteoblast MC3T3-E1 cells inside the hydrogels, the potential of the materials for bone tissue regeneration requires future analyses, for instance utilizing primary human osteoblast cells and eventually by conducting *in vivo* studies. Future work should include the detailed investigation of bone regeneration with time-dependent tissue-material interaction based on gene expression and histological evaluation of ADA-GEL/FS, to assess the effect of FS-incorporated ADA-GEL bioinks. Such future research will be designed to further specify the important hallmarks of ADA-GEL/FS—bone interaction, finally evaluating the success of the here presented bioink for *in vivo* bone TE using advanced models.

5. Conclusions

In this study, a bioink formulation composed of ADA-GEL and FS particles has been introduced as a promising candidate for bone regeneration. The effects of FS particle addition into the ADA-GEL matrix were investigated in terms of material characteristics, cytocompatibility, and osteogenic differentiation. FS particles were homogeneously distributed in the 3D-bioprinted hydrogels and showed suitable interaction with ADA-GEL. Mechanical properties were significantly improved, and it was found that the stiffness of the hydrogels is tunable with the incorporation of the particles. 3D bioprinted ADA-GEL/FS composite hydrogels exhibited bioactivity as well as a favorable microenvironment for MC3T3-E1 cells. Besides the nontoxicity of the bioink, FS particle incorporation increased cell proliferation and osteogenic differentiation of pre-osteoblast cells. Cytocompatibility, similar biochemical composition to bone, distinctive collagen fiber orientation, natural biomineralization capacity by hydroxyapatite content, and convenient printability make ADA-GEL/FS a promising biomaterial for bone TE. Besides, FS is a naturally derived waste material and can be obtained by a cost-effective process. With the successful fabrication of ADA-GEL/FS bioinks and their promising osteoinduction effectiveness, the use of FS particles in 3D bioprinting approaches provides biocompatible structures with suitable stiffness for potential bone regeneration applications.

Data availability statement

The data that support the findings of this study are available upon reasonable request from the authors.

Acknowledgments

This study was supported by The Scientific and Technology Research Council of Turkey (TUBITAK 2214-A, International Doctoral Research Fellowship Program) and Council of Higher Education of Turkey for 100/2000 PhD Scholarship in the field of Biomaterials and Tissue Engineering (CoHE 100/2000). In addition, the authors acknowledge İzmir Institute of Technology, Center for Materials Research (IZTECH MAM) for SEM analyses. We thank Professor Michael Gelinsky for granting access to his laboratory at TU Dresden (Germany) for the rheology measurements.

Author contributions

A K: conceptualization, methodology, investigation, material and experimental design, experiments, data analysis, writing of the original draft, review, and editing. T D: conceptualization, methodology, material and experimental design, review and editing. F T: conceptualization, methodology, review and editing, supervision. A R B: conceptualization, methodology, resources, review and editing, supervision.

ORCID iDs

Aylin Kara Özenler https://orcid.org/0000-0001-8302-913X
Thomas Distler https://orcid.org/0000-0002-0319-3763
Funda Tihminlioglu https://orcid.org/0000-0002-3715-8253
Aldo R Boccaccini https://orcid.org/0000-0002-7377-2955

References

[1] Murphy S V and Atala A 2014 3D bioprinting of tissues and organs *Nat. Biotechnol.* **32** 773–85
[2] Malda J, Visser J, Melchels F P, Jüngst T, Hennink W E, Dhert W J A, Groll J and Hutmacher D W 2013 25th anniversary article: engineering hydrogels for biofabrication *Adv. Mater.* **25** 5011–28
[3] Zadpoor A A and Malda J 2017 Additive manufacturing of biomaterials, tissues, and organs *Ann. Biomed. Eng.* **45** 1–11
[4] Groll J *et al* 2016 Biofabrication: reappraising the definition of an evolving field *Biofabrication* **8** 013001
[5] Fedorovich N E, Alblas J, De Wijn J R, Hennink W E, Verbout A B J and Dhert W J A 2007 Hydrogels as extracellular matrices for skeletal tissue engineering: state-of-the-art and novel application in organ printing *Tissue Eng.* **13** 1905–25
[6] Freeman F E and Kelly D J 2017 Tuning alginate bioink stiffness and composition for controlled growth factor delivery and to spatially direct MSC fate within bioprinted tissues *Sci. Rep.* **7** 17042
[7] Dinescu S, Albu Kaya M, Chitoiu L, Ignat S, Kaya D A and Costache M 2019 Collagen-based hydrogels and their applications for tissue engineering and regenerative medicine *Cellulose-Based Superabsorbent Hydrogels* (*Polymers and Polymeric Composites: A Reference Series*) ed M Mondal (Cham: Springer) pp 1643–64
[8] Hu P *et al* 2022 *In-situ* formable dextran/chitosan-based hydrogels functionalized with collagen and EGF for diabetic wounds healing *Biomater. Adv.* **136** 212773
[9] Montalbano G, Toumpaniari S, Popov A, Duan P, Chen J, Dalgarno K, Scott W E and Ferreira A M 2018 Synthesis of bioinspired collagen/alginate/fibrin based hydrogels for soft tissue engineering *Mater. Sci. Eng.* C **91** 236–46
[10] Narayan R, Agarwal T, Mishra D, Maiti T K and Mohanty S 2018 Goat tendon collagen-human fibrin hydrogel for comprehensive parametric evaluation of HUVEC microtissue-based angiogenesis *Colloids Surf.* B **163** 291–300
[11] Singh R, Sarker B, Silva R, Detsch R, Dietel B, Alexiou C, Boccaccini A R and Cicha I 2016 Evaluation of hydrogel matrices for vessel bioplotting: vascular cell growth and viability *J. Biomed. Mater. Res.* A **104** 577–85
[12] Chawla D, Kaur T, Joshi A and Singh N 2020 3D bioprinted alginate-gelatin based scaffolds for soft tissue engineering *Int. J. Biol. Macromol.* **141** 560–7
[13] Boontheekul T, Kong H J and Mooney D J 2005 Controlling alginate gel degradation utilizing partial oxidation and bimodal molecular weight distribution *Biomaterials* **26** 2455–65
[14] Distler T, McDonald K, Heid S, Karakaya E, Detsch R and Boccaccini A R 2020 Ionically and enzymatically dual cross-linked oxidized alginate gelatin hydrogels with tunable stiffness and degradation behavior for tissue engineering *ACS Biomater. Sci. Eng.* **6** 3899–914
[15] Sarker B, Singh R, Zehnder T, Forgber T, Alexiou C, Cicha I, Detsch R and Boccaccini A R 2017 Macromolecular interactions in alginate-gelatin hydrogels regulate the behavior of human fibroblasts *J. Bioact. Compat. Polym.* **32** 309–24
[16] Reakasame S and Boccaccini A R 2018 Oxidized alginate-based hydrogels for tissue engineering applications: a review *Biomacromolecules* **19** 3–21
[17] Kong X, Chen L, Li B, Quan C and Wu J 2021 Applications of oxidized alginate in regenerative medicine *J. Mater. Chem.* B **9** 2785–801
[18] Sharifi S *et al* 2021 Tuning gelatin-based hydrogel towards bioadhesive ocular tissue engineering applications *Bioact. Mater.* **6** 3947–61
[19] Wright B, De Bank P A, Luetchford K A, Acosta F R and Connon C J 2014 Oxidized alginate hydrogels as niche environments for corneal epithelial cells *J. Biomed. Mater. Res.* A **102** 3393–400
[20] Zehnder T, Sarker B, Boccaccini A R and Detsch R 2015 Evaluation of an alginate-gelatine crosslinked hydrogel for bioplotting *Biofabrication* **7** 025001
[21] Ruther F, Distler T, Boccaccini A R and Detsch R 2019 Biofabrication of vessel-like structures with alginate di-aldehyde—gelatin (ADA-GEL) bioink *J. Mater. Sci., Mater. Med.* **30** 8
[22] Kreller T, Distler T, Heid S, Gerth S, Detsch R and Boccaccini A R 2021 Physico-chemical modification of gelatine for the improvement of 3D printability of oxidized alginate-gelatine hydrogels towards cartilage tissue engineering *Mater. Des.* **208** 109877
[23] Labowska M B, Cierluk K, Jankowska A M, Kulbacka J, Detyna J and Michalak I 2021 A review on the adaption of alginate-gelatin hydrogels for 3D cultures and bioprinting *Materials* **14** 858
[24] Zhu H, Monavari M, Zheng K, Distler T, Ouyang L, Heid S, Jin Z, He J, Li D and Boccaccini A R 2022 3D bioprinting of multifunctional dynamic nanocomposite bioinks incorporating Cu-doped mesoporous bioactive glass nanoparticles for bone tissue engineering *Small* **18** 2194996
[25] Cai F F, Heid S and Boccaccini A R 2021 Potential of Laponite® incorporated oxidized alginate–gelatin (ADA-GEL) composite hydrogels for extrusion-based 3D printing *J. Biomed. Mater. Res.* B **109** 1090–104
[26] Sheffield C, Meyers K, Johnson E and Rajachar R M 2018 Application of composite hydrogels to control physical properties in tissue engineering and regenerative medicine *Gels* **4** 51
[27] Iglesias-Mejuto A and García-González C A 2021 3D-printed alginate-hydroxyapatite aerogel scaffolds for bone tissue engineering *Mater. Sci. Eng.* C **131** 112525
[28] Dutta S D, Hexiu J, Patel D K, Ganguly K and Lim K T 2021 3D-printed bioactive and biodegradable hydrogel scaffolds of alginate/gelatin/cellulose nanocrystals for tissue engineering *Int. J. Biol. Macromol.* **167** 644–58
[29] Lee M, Bae K, Guillon P, Chang J, Arlov Ø and Zenobi-Wong M 2018 Exploitation of cationic silica nanoparticles for bioprinting of large-scale constructs with high printing fidelity *ACS Appl. Mater. Interfaces* **10** 37820–8
[30] Nelson M, Li S, Page S J, Shi X, Lee P D, Stevens M M, Hanna J V and Jones J R 2021 3D printed silica-gelatin hybrid scaffolds of specific channel sizes promote collagen type II, Sox9 and aggrecan production from chondrocytes *Mater. Sci. Eng.* C **123** 111964
[31] Rencsok M, Stichler S, Böck T, Paxton N, Bertlein S, Levato R and Schill V 2017 Double printing of hyaluronic acid/poly(glycidol) hybrid hydrogels with poly ε-caprolactone) for MSC chondrogenesis *Biofabrication* **9** 044108
[32] Zhao X, Ding M, Xu C, Zhang X, Liu S, Lin X, Wang L and Xia Y 2021 A self-reinforcing strategy enables the intimate interface for anisotropic alginate composite hydrogels *Carbohydrate Polym.* **251** 117054
[33] Kim H S, Kim C and Lee K Y 2022 Three-dimensional bioprinting of polysaccharide-based self-healing hydrogels with dual cross-linking *J. Biomed. Mater. Res.* A **110** 761–72

[34] van Essen T H et al 2016 Biocompatibility of a fish scale-derived artificial cornea: cytotoxicity, cellular adhesion and phenotype, and in vivo immunogenicity Biomaterials 81 36–45
[35] Pon-On W, Suntornsaratoon P, Charoenphandhu N, Thongbunchoo J, Krishnamra N and Tang I M 2016 Hydroxyapatite from fish scale for potential use as bone scaffold or regenerative material Mater. Sci. Eng. C 62 183–9
[36] Ikoma T, Kobayashi H, Tanaka J, Walsh D and Mann S 2003 Microstructure, mechanical, and biomimetic properties of fish scales from Pagrus major J. Struct. Biol. 142 327–33
[37] Okuda M, Ogawa N, Takeguchi M, Hashimoto A, Tagaya M, Chen S, Hanagata N and Ikoma T 2011 Minerals and aligned collagen fibrils in tilapia fish scales: structural analysis using dark-field and energy-filtered transmission electron microscopy and electron tomography Microsc. Microanal. 17 788–98
[38] Murcia S, Ghods S, Ossa A and Arola D 2022 Tuning protecto-flexibility in nature: case of the fish scale Nat. Sci. 2 20210097
[39] Fang Z, Wang Y, Feng Q, Kienzle A and Müller W E G 2014 Hierarchical structure and cytocompatibility of fish scales from Carassius auratus Mater. Sci. Eng. C 43 145–57
[40] Lin C C, Ritch R, Lin S M, Ni M H, Chang Y C, Lu Y L, Lai H J and Lin F H 2010 A new fish scale-derived scaffold for corneal regeneration Eur. Cells Mater. 26 50–57
[41] Sackett S D et al 2018 Extracellular matrix scaffold and hydrogel derived from decellularized and delipidized human pancreas Sci. Rep. 8 10452
[42] Kaczmarek B, Sionkowska A and Osyczka A M 2017 Collagen-based scaffolds enriched with glycosaminoglycans isolated from skin of Salmo salar fish Polym. Test. 62 132–6
[43] Yamamoto K, Igawa K, Sugimoto K, Yoshizawa Y, Yanagiguchi K, Ikeda T, Yamada S and Hayashi Y 2014 Biological safety of fish (tilapia) collagen Biomed. Res. Int. 2014 630757
[44] Jana P, Mitra T, Selvaraj T K R, Gnanamani A and Kundu P P 2016 Preparation of guar gum scaffold film grafted with ethylenediamine and fish scale collagen, cross-linked with ceftazidime for wound healing application Carbohydrate Polym. 153 573–81
[45] Mondal S, Pal U and Dey A 2016 Natural origin hydroxyapatite scaffold as potential bone tissue engineering substitute Ceram. Int. 42 18338–46
[46] Choi D J et al 2015 Bioactive fish collagen/polycaprolactone composite nanofibrous scaffolds fabricated by electrospinning for 3D cell culture J. Biotechnol. 10 47–58
[47] Chou C-H, Chen Y-G, Lin -C-C, Lin S-M, Yang K-C and Chang S-H 2014 Bioabsorbable fish scale for the internal fixation of fracture: a preliminary study Tissue Eng. A 20 2493–502
[48] Kara A, Tamburaci S, Tihminlioglu F and Havitcioglu H 2019 Bioactive fish scale incorporated chitosan biocomposite scaffolds for bone tissue engineering Int. J. Biol. Macromol. 130 266–79
[49] Wu W, Zhou Z, Sun G, Liu Y, Zhang A and Chen X 2021 Construction and characterization of degradable fish scales for enhancing cellular adhesion and potential using as tissue engineering scaffolds Mater. Sci. Eng. C 122 111919
[50] Kara A, Gunes O C, Albayrak A Z, Bilici G, Erbil G and Havitcioglu H 2020 Fish scale/poly(3-hydroxybutyrate-co-3-hydroxyvalerate) nanofibrous composite scaffolds for bone regeneration J. Biomater. Appl. 34 1201–15
[51] Boonyagul S, Pukasamsombut D, Pengpanich S, Toobunterng T, Pasanaphong K, Sathirapongsasuti N, Tawonsawatruk T, Wangtueai S and Tanadchangsaeng N 2022 Bioink hydrogel from fish scale gelatin blended with alginate for 3D-bioprinting application J. Food Process. Preserv. 46 e15864
[52] Soltan N, Ning L, Mohabatpour F, Papagerakis P and Chen X 2019 Printability and cell viability in bioprinting alginate dialdehyde-gelatin scaffolds ACS Biomater. Sci. Eng. 5 2976–87
[53] Dranseikiene D, Schrüfer S, Schubert D W, Reakasame S and Boccaccini A R 2020 Cell-laden alginate dialdehyde–gelatin hydrogels formed in 3D printed sacrificial gel J. Mater. Sci., Mater. Med. 31 31
[54] Ouyang L, Yao R, Zhao Y and Sun W 2016 Effect of bioink properties on printability and cell viability for 3D bioplotting of embryonic stem cells Biofabrication 8 035020
[55] Chaudhuri O et al 2016 Hydrogels with tunable stress relaxation regulate stem cell fate and activity Nat. Mater. 15 326–34
[56] Kokubo T and Takadama H 2006 How useful is SBF in predicting in vivo bone bioactivity? Biomaterials 27 2907–15
[57] Muyonga J H, Cole C G B and Duodu K G 2004 Fourier transform infrared (FTIR) spectroscopic study of acid soluble collagen and gelatin from skins and bones of young and adult Nile perch (Lates niloticus) Food Chem. 86 325–32
[58] Qin D, Bi S, You X, Wang M, Cong X, Yuan C, Yu M, Cheng X and Chen X G 2022 Development and application of fish scale wastes as versatile natural biomaterials Chem. Eng. J. 428 131101
[59] Feng X, Zhang X, Li S, Zheng Y, Shi X, Li F, Guo S and Yang J 2020 Preparation of aminated fish scale collagen and oxidized sodium alginate hybrid hydrogel for enhanced full-thickness wound healing Int. J. Biol. Macromol. 164 626–37
[60] Heid S, Becker K, Byun J, Biermann I, Neščáková Z, Zhu H, Groll J and Boccaccini A R 2022 Bioprinting with bioactive alginate dialdehyde-gelatin (ADA-GEL) composite bioinks: time-dependent in-situ crosslinking via addition of calcium-silicate particles tunes in vitro stability of 3D bioprinted constructs Bioprinting 26 e00200
[61] Piez K A and Gross J 1960 The amino acid composition of some fish collagens: the relation between composition and structure J. Biol. Chem. 235 995–8
[62] Alcaide-Ruggiero L, Molina-Hernández V, Granados M M and Domínguez J M 2021 Main and minor types of collagens in the articular cartilage: the role of collagens in repair tissue evaluation in chondral defects Int. J. Mol. Sci. 22 13329
[63] Subhan F, Kang H Y, Lim Y, Ikram M, Baek S Y, Jin S, Jeong Y H, Kwak J Y and Yoon S 2017 Fish scale collagen peptides protect against $CoCl_2$/TNF- α-induced cytotoxicity and inflammation via inhibition of ROS, MAPK, and NF-κ B pathways in HaCaT cells Oxid. Med. Cell. Longevity 2017 9703609
[64] Zoch M L, Clemens T L and Riddle R C 2016 New insights into the biology of osteocalcin Bone 82 42–49
[65] Xia H, Dong L, Hao M, Wei Y, Duan J, Chen X, Yu L, Li H, Sang Y and Liu H 2021 Osteogenic property regulation of stem cells by a hydroxyapatite 3D-hybrid scaffold with cancellous bone structure Front. Chem. 9 798299
[66] Alipour M, Firouzi N, Aghazadeh Z, Samiei M, Montazersaheb S, Khoshfetrat A B and Aghazadeh M 2021 The osteogenic differentiation of human dental pulp stem cells in alginate-gelatin/nano-hydroxyapatite microcapsules BMC Biotechnol. 21 6
[67] Liang H, Xu X, Feng X, Ma L, Deng X, Wu S, Liu X and Yang C 2019 Gold nanoparticles-loaded hydroxyapatite composites guide osteogenic differentiation of human mesenchymal stem cells through Wnt/β-catenin signaling pathway Int. J. Nanomed. 2 6151–63
[68] Liu C and Sun J 2014 Potential application of hydrolyzed fish collagen for inducing the multidirectional differentiation of rat bone marrow mesenchymal stem cells Biomacromolecules 15 436–43
[69] Grigorakis K 2007 Compositional and organoleptic quality of farmed and wild gilthead sea bream (Sparus aurata) and sea bass (Dicentrarchus labrax) and factors affecting it: a review Aquaculture 272 57–75
[70] Domínguez D, Robaina L, Zamorano M J, Karalazos V and Izquierdo M 2019 Effects of zinc and manganese sources on

gilthead seabream (Sparus aurata) fingerlings *Aquaculture* **505** 386–92
[71] Mohanty B *et al* 2014 Amino acid compositions of 27 food fishes and their importance in clinical nutrition *J. Amino Acids* **2014** 269797
[72] Zhuang J, Lin S, Dong L, Cheng K and Weng W 2018 Magnetically actuated mechanical stimuli on Fe_3O_4/mineralized collagen coatings to enhance osteogenic differentiation of the MC3T3-E1 cells *Acta Biomater.* **15** 49–60
[73] Stanton A E, Tong X, Lee S and Yang F 2019 Biochemical ligand density regulates yes-associated protein translocation in stem cells through cytoskeletal tension and integrins *ACS Appl. Mater. Interfaces* **11** 8849–57
[74] Bertrand A A, Malapati S H, Yamaguchi D T and Lee J C 2020 The intersection of mechanotransduction and regenerative osteogenic materials *Adv. Healthcare Mater.* **9** 2000709
[75] Silver F H and Siperko L M 2003 Mechanosensing and mechanochemical transduction: how is mechanical energy sensed and converted into chemical energy in an extracellular matrix? *Crit. Rev. Biomed. Eng.* **31** 255–331
[76] Liu N, Zhou M, Zhang Q, Yong L, Zhang T, Tian T, Ma Q, Lin S, Zhu B and Cai X 2018 Effect of substrate stiffness on proliferation and differentiation of periodontal ligament stem cells *Cell Prolif.* **51** e12478
[77] Khatiwala C B, Kim P D, Peyton S R and Putnam A J 2009 ECM compliance regulates osteogenesis by influencing MAPK signaling downstream of RhoA and ROCK *J. Bone Miner. Res.* **24** 886–98
[78] Ahlfeld T, Cidonio G, Kilian D, Duin S, Akkineni A R, Dawson J I, Yang S, Lode A, Oreffo R O C and Gelinsky M 2017 Development of a clay based bioink for 3D cell printing for skeletal application *Biofabrication* **9** 034103
[79] Gelinsky M and Ahlfeld T 2022 Additive manufacturing of polymers and ceramics for tissue engineering applications *Tissue Engineering Using Ceramics and Polymers* ed A R Boccaccini, P X Ma and L Liverani (Sawston: Woodhead Publishing) pp 385–406